RESEARCH ARTICLE

CRISPR-Cas9-Mediated Single-Gene and Gene Family Disruption in *Trypanosoma cruzi*

Duo Peng,[a,b] Samarchith P. Kurup,[a,b]* Phil Y. Yao,[a,b] Todd A. Minning,[a,b] Rick L. Tarleton[a,b]

Center for Tropical and Emerging Global Diseases[a] and Department of Cellular Biology,[b] University of Georgia, Athens, Georgia, USA

* Present address: Samarchith P. Kurup, Department of Microbiology, University of Iowa, Iowa City, Iowa, USA.

ABSTRACT ***Trypanosoma cruzi* is a protozoan parasite of humans and animals, affecting 10 to 20 million people and innumerable animals, primarily in the Americas. Despite being the largest cause of infection-induced heart disease worldwide, even among the neglected tropical diseases (NTDs) *T. cruzi* is considered one of the least well understood and understudied. The genetic complexity of *T. cruzi* as well as the limited set of efficient techniques for genome engineering contribute significantly to the relative lack of progress in and understanding of this pathogen. Here, we adapted the CRISPR-Cas9 system for the genetic engineering of *T. cruzi*, demonstrating rapid and efficient knockout of multiple endogenous genes, including essential genes. We observed that in the absence of a template, repair of the Cas9-induced double-stranded breaks (DSBs) in *T. cruzi* occurs exclusively by microhomology-mediated end joining (MMEJ) with various-sized deletions. When a template for DNA repair is provided, DSB repair by homologous recombination is achieved at an efficiency several orders of magnitude higher than that in the absence of CRISPR-Cas9-induced DSBs. We also demonstrate the high multiplexing capacity of CRISPR-Cas9 in *T. cruzi* by knocking down expression of an enzyme gene family consisting of 65 members, resulting in a significant reduction of enzymatic product with no apparent off-target mutations. Lastly, we show that Cas9 can mediate disruption of its own coding sequence, rescuing a growth defect in stable Cas9-expressing parasites. These results establish a powerful new tool for the analysis of gene functions in *T. cruzi*, enabling the study of essential genes and their functions and analysis of the many large families of related genes that occupy a substantial portion of the *T. cruzi* genome.**

IMPORTANCE ***Trypanosoma cruzi*, the causative agent of human Chagas disease, is the leading worldwide cause of infectious myocarditis. Diagnostics for the infection are relatively poor, treatment options are limited and of variable effectiveness, and suitable vaccines are nonexistent. The *T. cruzi* genome is replete with genes of unknown function and greatly expanded gene families with hundreds of members. The absence of facile genetic engineering tools, including RNA interference, for *T. cruzi* has prevented elucidation of gene and gene family function and the development of better infection prevention and control measures. In this study, we demonstrate that the CRISPR-Cas9 system is a versatile and powerful tool for genome manipulations in *T. cruzi*, bringing new opportunities for unraveling the functions of previously uncharacterized genes and how this human pathogen engages its large families of genes encoding surface proteins to interact with human and animal hosts.**

Received 6 October 2014 **Accepted** 25 November 2014 **Published** 30 December 2014

Citation Peng D, Kurup SP, Yao PY, Minning TA, Tarleton RL. 2015. CRISPR-Cas9-mediated single-gene and gene family disruption in *Trypanosoma cruzi*. mBio 6(1):e02097-14. doi:10.1128/mBio.02097-14.

Editor Patricia J. Johnson, UCLA

Address correspondence to Rick L. Tarleton, tarleton@uga.edu.

The protozoan parasite *Trypanosoma cruzi* is the causative agent of Chagas disease, the highest-impact infectious disease of the Americas, with 10 to 20 million humans and innumerable animals affected. The study of *T. cruzi* and Chagas disease is particularly challenging, in part due to the complexity and unique characteristics of its genome and the relative paucity of tools for manipulation of these characteristics and thus determine their importance for parasite persistence and pathogenicity. In addition to the substantial number of genes lacking homologues in other eukaryotes, the *T. cruzi* genome also contains an unprecedented number of gene families, in some cases families with thousands of members (1–3). Among the largest of these gene families are those encoding *trans*-sialidase-like proteins, mucins, and mucin-associated proteins that are expressed on the parasite surface and thus directly interact with insect and animal hosts—including interactions as immunological targets.

Although methods to express exogenous genes or overexpress endogenous genes and to delete genes in *T. cruzi* have proven useful, these methods are laborious and time-consuming. For example, current gene knockout (KO) strategies utilize spontaneous homologous recombination of a DNA cassette containing a drug selection marker generally flanked by ~500 bp of coding sequence (CDS) or untranslated regions (UTRs) of the target gene. In addition to the fact that homologous recombination in *T. cruzi* has a very low efficiency, this approach is limited to a single-allele KO per drug selection marker (4), and the drug selection process is slow, requiring at least 1 month per allele. Collectively, the success rate for generating null mutants in *T. cruzi* is low, and the limited

number of drug-selectable markers restricts the number of manipulations that can be attempted in a single organism. These constraints, in combination with the absence of a functional RNA interference (RNAi) system in *T. cruzi*, make virtually unapproachable the manipulation of multigene families and the determination of how gene family sizes are generated, maintained, and contribute to parasite success in *T. cruzi*.

A system with RNA-guided nucleases utilizing clustered, regularly interspaced, short palindromic repeats, the CRISPR-associated (CRISPR-Cas) nuclease system, has enabled rapid, targeted modification of a wide range of genomes (5). The system has proven especially useful because of its relative ease and high efficiency, as well as the ability to achieve multiple modifications in a single organism/cell (6). The specificity and targeted genome editing by CRISPR-Cas9 is achieved by a guide RNA that directs the Cas9 protein to genome locations by RNA-DNA hybridization, introducing a double-stranded break (DSB). In most species, the repair of the DSBs occurs by a nonhomologous end-joining (NHEJ) pathway, creating insertions or deletions (indels) or, if in the presence of an appropriate DNA template, by homologous recombination.

Here we report the use of the CRISPR-Cas9 system in *T. cruzi* to knock out target genes and to enhance gene insertion by homologous recombination. Gene disruption is highly efficient, with up to 70% of the population exhibiting a mutant phenotype, and rapid, with decreased protein levels evident as early as 2 days after transfection. Because of these qualities, observation of the impact of disruption of essential genes was possible, with an efficiency rivaling that of RNAi. In the absence of a template, repair of the Cas9-induced DSBs in *T. cruzi* occurs exclusively by microhomology-mediated end joining (MMEJ) with various-sized deletions, depending on the locations of the homologous regions. The latter finding confirms the apparent absence of NHEJ and the dominance of MMEJ repair mechanisms in kinetoplastids (7, 8). Finally, we provide proof of concept that the CRISPR-Cas9 system can be multiplexed to knock out multiple genes in a large (>50-member) gene family, with no apparent off-target mutations. These results establish a powerful new tool for genome manipulation in *T. cruzi* and open the door to greater understanding of the roles of essential genes and large gene families in the biology of this human pathogen and its interactions with its animal hosts.

RESULTS

High-frequency Cas9-sgRNA-mediated gene disruption in *T. cruzi*. To determine the ability of single guide RNA (sgRNA) of Cas9 to disrupt genes in *T. cruzi*, we first stably expressed both enhanced green fluorescent protein (eGFP) and Cas9 in *T. cruzi* by using separate pTrex backbone plasmids (9) under G418 and blasticidin drug selection, respectively (Fig. 1A). Transfection of epimastigotes of *T. cruzi* with sgRNA, which was previously shown to mediate eGFP disruption in human cell lines (10), resulted in rapid and highly efficient reduction in GFP expression. Each of the three sgRNAs induced loss of GFP in ~50 to 60% of parasites as early as day 2 after transfection (Fig. 1B), No reduction in eGFP expression was observed in epimastigotes transfected with 80-bp human 18S rRNA as a control. GFP-targeted sgRNAs were also very efficient at disrupting gene expression when electroporated into trypomastigotes of *T. cruzi*, with Vero cells infected with recently transfected trypomastigotes showing a mixture of GFP-positive and GFP-negative parasites 5 days after transfection/infection (Fig. 1D).

Although the Cas9-mediated mutation of GFP was highly efficient, 40% or more of the population of parasites transfected with sgRNA showed no change in GFP expression levels. Simultaneous (see Fig. S1 in the supplemental material) or serial (see Fig. S2 in the supplemental material) transfection with multiple GFP-directed guides only modestly increased the frequency of eGFP mutations above that from a single guide. Additionally, increasing the concentration of sgRNA to >10 μg/10^7 parasites failed to impact the frequency of eGFP mutants (see Fig. S3 in the supplemental material). To determine if this "resistance" to Cas9-mediated mutation might be linked to Cas9 protein levels, we used fluorescence-activated cell sorting to analyze the GFP-positive and GFP-negative parasites following transfection with the eGFP sgRNA, and we measured Cas9 levels in an enzyme-linked immunosorbent assay (ELISA). On average, the GFP-positive parasites had significantly lower levels of Cas9 protein than parasites in which GFP was disrupted by sgRNA transfection (Fig. 1C), suggesting that the less-than-100% efficiency of gene disruption in this system is due to low and variable levels of Cas9 expression.

sgRNA-guided Cas9 mutation of endogenous genes. In order to validate the use of CRISPR-Cas9 to mutate endogenous genes, we designed sgRNA targeting a number of *T. cruzi* genes by using a custom sgRNA design tool that selects sgRNA based in part on the absence of predicted off-targets (available at http://grna.ctegd.uga.edu). Transfection of *T. cruzi* epimastigotes or trypomastigotes with sgRNA targeting the multicopy α-tubulin genes resulted in parasites with misshapen and enlarged cell bodies and multiple flagella (Fig. 2A and B). Similar defects in cytokinesis and cell shape were previously reported following RNAi-mediated knockdown of α-tubulin in *Trypanosoma brucei* (11).

To better estimate the efficiency of endogenous gene knockout using sgRNA-guided Cas9, we performed transfection of sgRNA targeting single-locus genes encoding histidine ammonia lyase (HAL), an enzyme in the histidine metabolism pathway whose enzymatic activity can be easily quantified, and the putative fatty acid transporter (FATP) gene, whose protein actively can be monitored by uptake of BODIPY-labeled fatty acids. Epimastigotes transfected with the HAL sgRNA exhibited a 60% decrease in HAL activity at day 4 posttransfection compared to parasites transfected with the control 18s RNA (Fig. 2C). The epimastigotes were cloned by limiting dilution and assayed for HAL activity. Of the four clones tested, three exhibited no HAL activity, suggesting KO of both HAL alleles, and one (B6) demonstrated HAL activity similar to epimastigotes transfected with control 18s RNA. sgRNA-guided Cas9 targeting of FATP resulted in a 37% decrease in the fatty acid uptake rate (Fig. 2D). Our previous attempts to generate null mutants in FATP by conventional knockout strategies failed (4), indicating that the null mutation of FATP in *T. cruzi* is probably lethal. Indeed, examination of FA import activity in FATP-sgRNA parasites at 2 weeks posttransfection showed a near-normal FA uptake rate, suggesting the loss of the FATP mutant population and survival of only the nonmutated wild-type (WT) population. Thus, the high efficiency of the CRISPR-Cas9 system in *T. cruzi* allows for the study of loss of function over time due to the disruption of essential genes.

MMEJ-mediated repair of CRISPR-Cas9-induced DSBs in *T. cruzi*. Double-stranded DNA breaks induced by guided nucleases such as Cas9 are generally repaired in one of two ways: by

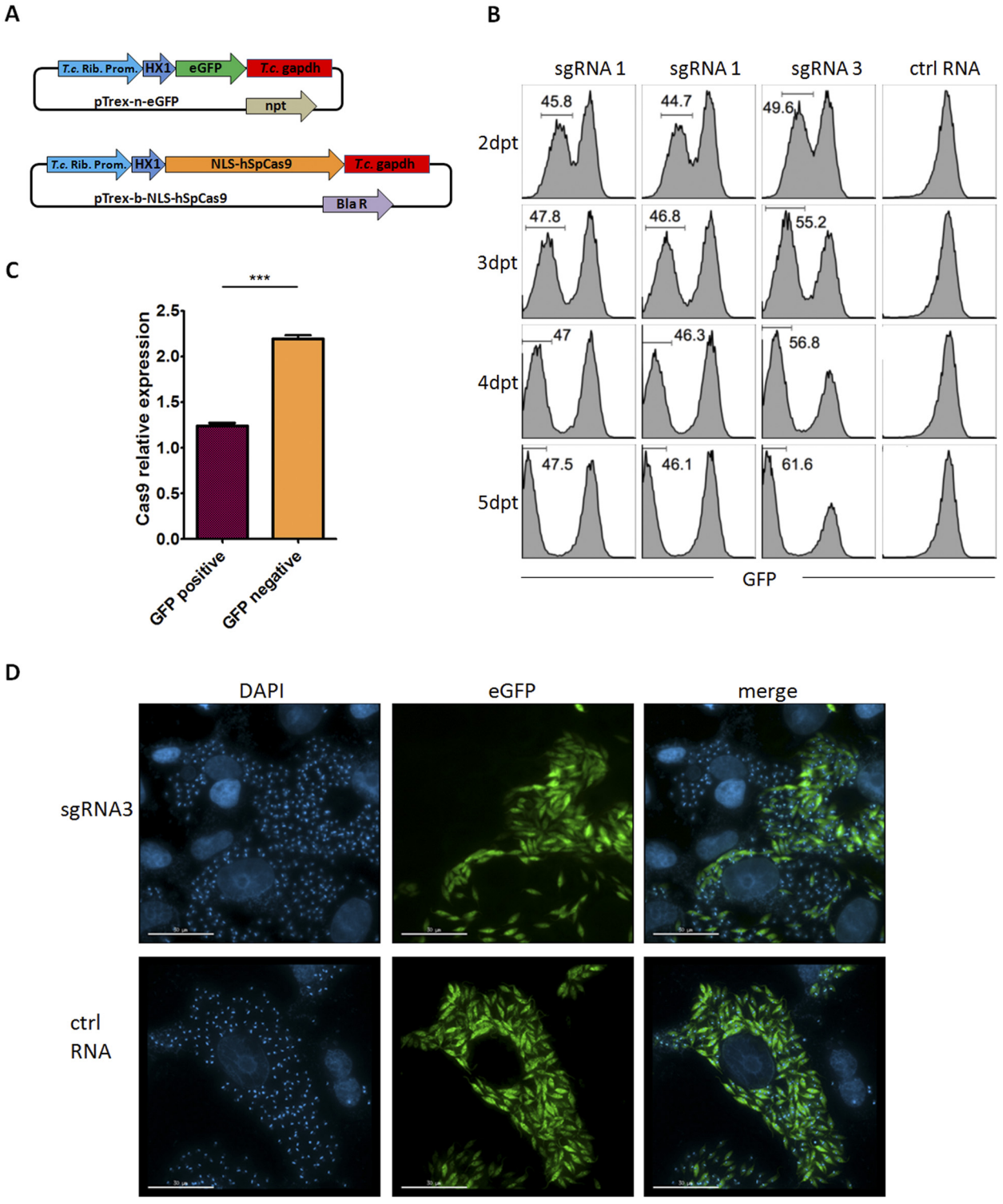

FIG 1 Cas9-mediated eGFP disruption in *T. cruzi* epimastigotes and trypomastigotes. (A) Design of constructs for stable expression of eGFP and nucleus-localized Cas9 in *T. cruzi*. (B) Flow cytometric analysis results for *T. cruzi* eGFP- and Cas9-expressing epimastigotes transfected with eGFP sgRNA. Disruption of eGFP was evident as early as 2 days posttransfection (dpt), and progressive loss of the GFP signal was observed over time. (C) ELISA analysis results for Cas9 expression in GFP-positive (eGFP-intact parasites [sequence confirmed]) and GFP-negative (Cas9-induced KO) parasites sorted following eGFP disruption. Expression levels of Cas9 were normalized to α-tubulin expression in corresponding samples. (D) eGFP- and Cas9-expressing *T. cruzi* trypomastigotes transfected with eGFP sgRNA or control RNA and then used to infect Vero cells and imaged 5 days later. Comparison of 4′,6-diamidino-2-phenylindole (DAPI)-stained nuclei and kinetoplasts with GFP fluorescence demonstrated a mixture of GFP-expressing and nonexpressing parasites in the eGFP-targeting sgRNA-transfected group and uniform GFP expression in parasites transfected with control RNA.

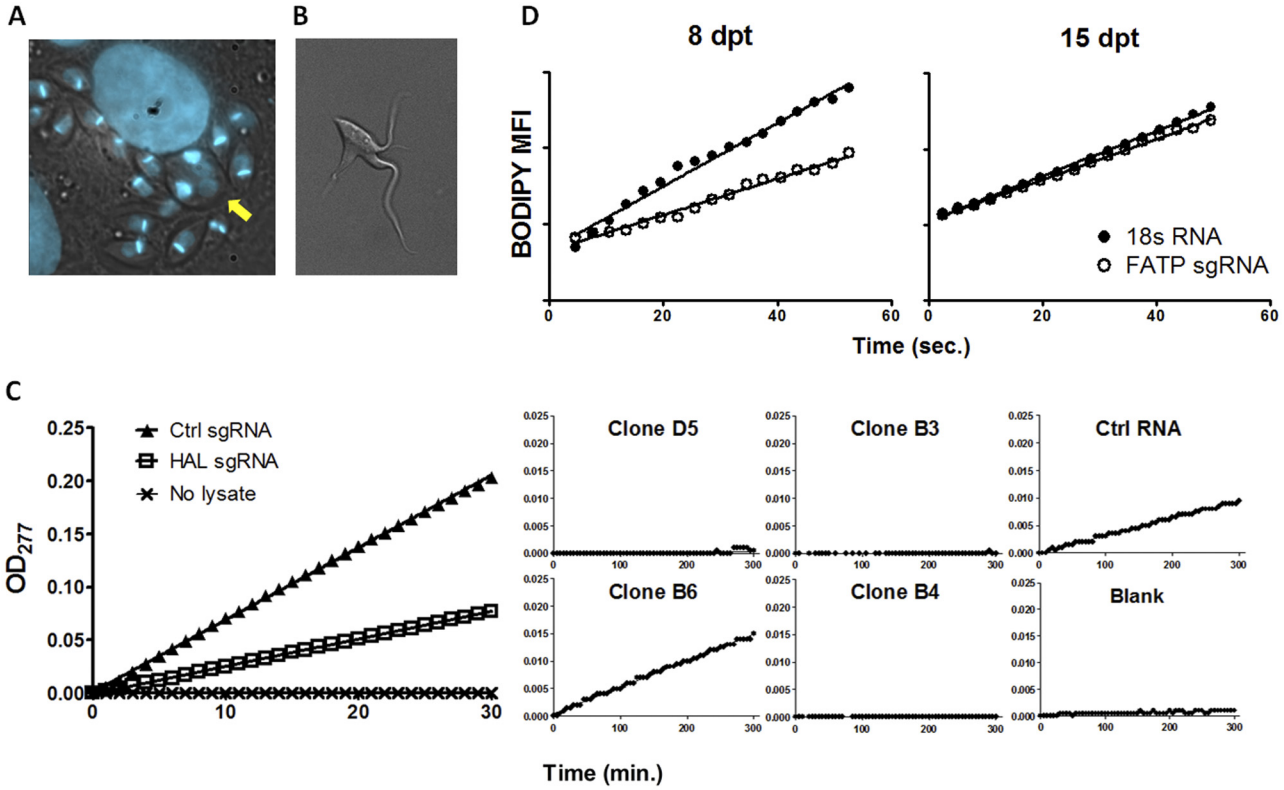

FIG 2 Disruption of endogenous *T. cruzi* genes by Cas9-mediated mutation. (A) 4′,6-Diamidino-2-phenylindole-stained Cas9-expressing *T. cruzi* trypomastigotes were transfected with α-tubulin-targeting sgRNA, used to infect Vero cells, and imaged 4 days later. Note the enlarged intracellular amastigote with multiple nuclei (arrow). (B) Swollen and multiflagellated Cas9-expressing *T. cruzi* epimastigote transfected with α-tubulin-targeting sgRNA. (C) HAL activity determined by the rate of urocanic acid formation (measured as the optical density at 277 nm) in epimastigote lysates 4 days posttransfection of HAL gene-targeting sgRNA or control (Ctrl) RNA. (Left) HAL activity of the transfected population; (right) HAL activity of individual clonal lines. Epimastigotes transfected with the HAL sgRNA exhibited a 60% decrease in HAL activity at day 4 posttransfection compared to parasites transfected with the control 18s RNA. Three of the four clones tested exhibited no HAL activity. (D) BODIPY-labeled fatty acid analogue uptake by epimastigotes at days 8 and 15 posttransfection with FATP (fatty acid transporter) gene-targeting sgRNA or control RNA. sgRNA-guided Cas9 targeting of FATP resulted in a 37% decrease in the fatty acid uptake rate at day 8, but at 2 weeks posttransfection, near-normal FA uptake was observed, suggesting the loss of the FATP mutant population and survival of only the nonmutated WT population.

error-prone NHEJ, resulting in indels of various sizes, or by homology-directed repair, which allows precise editing, from point mutations to large indels, depending on the available template. Sequencing of the eGFP gene from eGFP-negative clones produced by eGFP sequence-guided Cas9 DSBs showed a consistent 33-bp deletion at the sgRNA targeting site (Fig. 3). Although the deletion junctions occurred at slightly different positions, they all fell between a pair of homologous sequences of 10 bp flanking the cut site (Fig. 3, red highlight). This pattern is consistent with MMEJ pathway repair of DSBs in *T. cruzi*. Sequencing of the GFP gene from clones of the eGFP sgRNA-transfected population that remained GFP positive (Fig. 3) showed an intact GFP sequence, again consistent with insufficient Cas9-mediated DSBs in some parasites (data not shown).

Cas9-facilitated homologous recombination. Template-mediated repair of sgRNA-guided Cas9 cuts has been used to facilitate homology-directed repair (HDR) (12–16). In the presence of template DNA with sufficient homologous flanking sequences, homologous recombination can be induced in *T. cruzi* and has been extensively used for deletion of specific genes (4). However, this process appears to have very low efficiency and requires ~30 days of drug selection to obtain stable recombinants. To determine if sgRNA-guided Cas9 cuts could be used to achieve higher rates of homologous recombination in *T. cruzi*, we conducted a fluorescence marker swap assay. *T. cruzi* epimastigotes harboring an eGFP expression cassette were cotransfected with both a sgRNA targeting eGFP and a tdTomato expression cassette with 5′ and 3′ homology to the eGFP insert (Fig. 4A). As expected from the high rate of mutation observed with eGFP and other endogenous genes, the sgRNA transfection resulted in a predominant loss of eGFP fluorescence (Fig. 4B). However, the sgRNA targeting eGFP at the position from bp 100 and 152, respectively, yielded a 0.11% and 0.069% rate of fluorescence marker swap. In stark contrast, in the absence of the eGFP-targeted sgRNA (but in the presence of the tdTomato template), homologous recombination was below the level of detection by this assay.

Cas9 nickase (Cas9n), a mutant form of Cas9 which cuts only a single strand of the double-stranded DNA, has been successfully used in other organisms to favor gene repair by HDR over the production of mutations commonly produced by NHEJ repair of DSBs (17). However, transfection of neither a single nor double sgRNA (at eGFP positions 313 and 339) into Cas9 nickase-

```
eGFP          ATGCCACCTACGGCAAGCTGACCCTGAAGTTCATCTGCACCACCGGCAAGCTGCCCGTGCCCTGG
neg_clone 1   ATGCCACCTACGGCAA----------------------------------GCTGCCCGTGCCCTGG
neg_clone 2   ATGCCACCTACGGCAA----------------------------------GCTGCCCGTGCCCTGG
neg_clone 4   ATGCCACCTACGGCAAGCTGA------------------------------CCGTGCCCTGG
neg_clone 5   ATGCCACCTACGGCAA----------------------------------GCTGCCCGTGCCCTGG
neg_clone 6   ATGCCACCT-------------------------------CCGGCAAGCTGCCCGTGCCCTGG
neg_clone 8   ATGCCACCTACGGCAA----------------------------------GCTGCCCGTGCCCTGG
neg_clone 9   ATGCCACC--------------------------------ACCGGCAAGCTGCCCGTGCCCTGG
neg_clone 10  ATGCCACC--------------------------------ACCGGCAAGCTGCCCGTGCCCTGG

eGFP          ATGCCACCTACGGCAAGCTGACCCTGAAGTTCATCTGCACCACCGGCAAGCTGCCCGTGCCCTGG
neg_clone 1   ATGCCACCTACGGCAAGCTGACCCTGAAGTTCATCTGCACCACGG-CAAGCTGCCCGTGCCCTGG
neg_clone 2   ATGCCACCTACGGCAA----------------------------------GCTGCCCGTGCCCTGG
neg_clone 3   ATGCCACCTACGGCAA----------------------------------GCTGCCCGTGCCCTGG
neg_clone 4   ATGCCACCTACGGCAA----------------------------------GCTGCCCGTGCCCTGG
neg_clone 5   ATGCCACCTACGGCAA----------------------------------GCTGCCCGTGCCCTGG
neg_clone 6   ATGCCACCTACGGCAA----------------------------------GCTGCCCGTGCCCTGG
neg_clone 7   ATGCCACCTACGGCAA----------------------------------GCTGCCCGTGCCCTGG
neg_clone 9   ATGCCACCTACGGCAA----------------------------------GCTGCCCGTGCCCTGG
neg_clone 10  ATGCCACCTACGGCAA----------------------------------GCTGCCCGTGCCCTGG
```

FIG 3 Sequencing of the eGFP gene in GFP-disrupted clones sorted from parasite populations transfected with eGFP-targeting sgRNA 3 (top) and sgRNA 1 (bottom). Underlined is the sgRNA targeting sequence, the PAM is boxed (on the reverse strand), red marks show microhomology sequences flanking the sgRNA targeting sequence, and double-stranded cut sites are indicated with blue arrows. The sequence of negative clone 1 in the sgRNA-1 set (bottom) shows a single-base deletion in this region, likely due to a spontaneous mutation in GFP. All other sequences showed a 33-bp deletion; although deletion junctions occurred at slightly different positions, they all fell between a pair of homologous sequences of 10 bp flanking the cut site, as predicted by repair via an MMEJ pathway.

expressing epimastigotes of *T. cruzi* produced detectable replacement of eGFP with the supplied tdTomato template (see Fig. S4 and S5 in the supplemental material).

Mutation of a multigene family in *T. cruzi*. In addition to the time required to knock out multiple alleles in *T. cruzi* using conventional homologous recombination with drug-selectable markers (4), the genetic manipulation of *T. cruzi* is also challenging because of the high proportion of genes within moderate to large families (1). The success with the apparent disruption of multiple α-tubulin genes (*T. cruzi* is thought to have 10 to 18 loci for α-tubulin) prompted us to test if RNA-guided Cas9 could disrupt larger gene families in *T. cruzi*. For this purpose, we selected the β-galactofuranosyl glycosyltransferase (β-GalGT) family of 65 annotated genes (see Table S3 in the supplemental material). Members of this gene family share an average of 93.1% nucleotide sequence homology, making it possible to target the whole gene

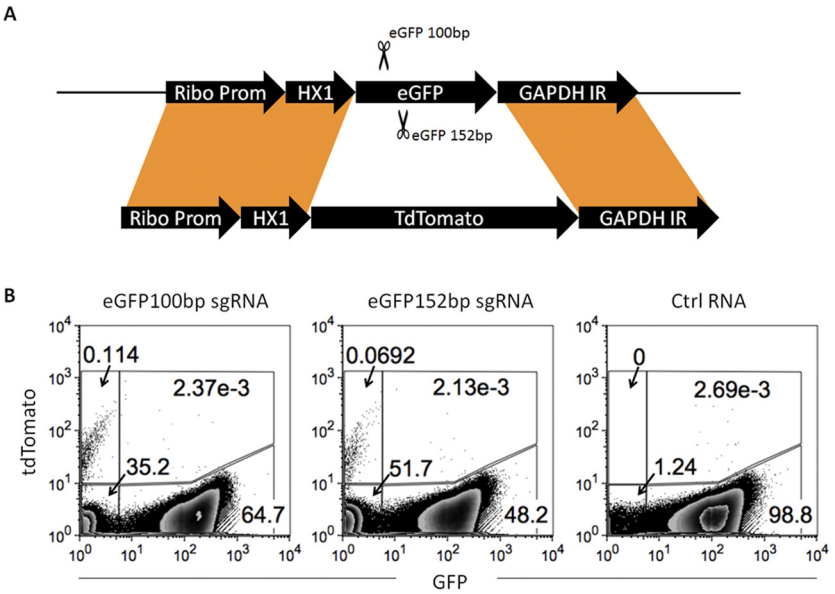

FIG 4 Homologous recombination-mediated replacement of the eGFP gene with a tdTomato gene facilitated by Cas9-induced DSBs in eGFP. (A) Schematic diagram of the fluorescence marker swap assay design. *T. cruzi* epimastigotes harboring an eGFP expression cassette were cotransfected with both a sgRNA targeting eGFP at position bp 100 or 152 and a tdTomato expression cassette with 5′ and 3′ homologies to the eGFP insert. (B) Flow cytometric analysis of tdTomato-eGFP fluorescence marker swap performed in Cas9-expressing epimastigotes 5 days after transfection with the indicated eGFP-targeting sgRNAs. Numbers indicate percentages of cells in each quadrant. The sgRNA targeting eGFP at position bp 100 and 152 , respectively, yielded a 0.11% and 0.069% rate of fluorescence marker swap, indicated by the loss of GFP and gain of tdTomato. In the absence of the eGFP-targeted sgRNA (but in the presence of the tdTomato template), homologous recombination was below the level of detection by this assay.

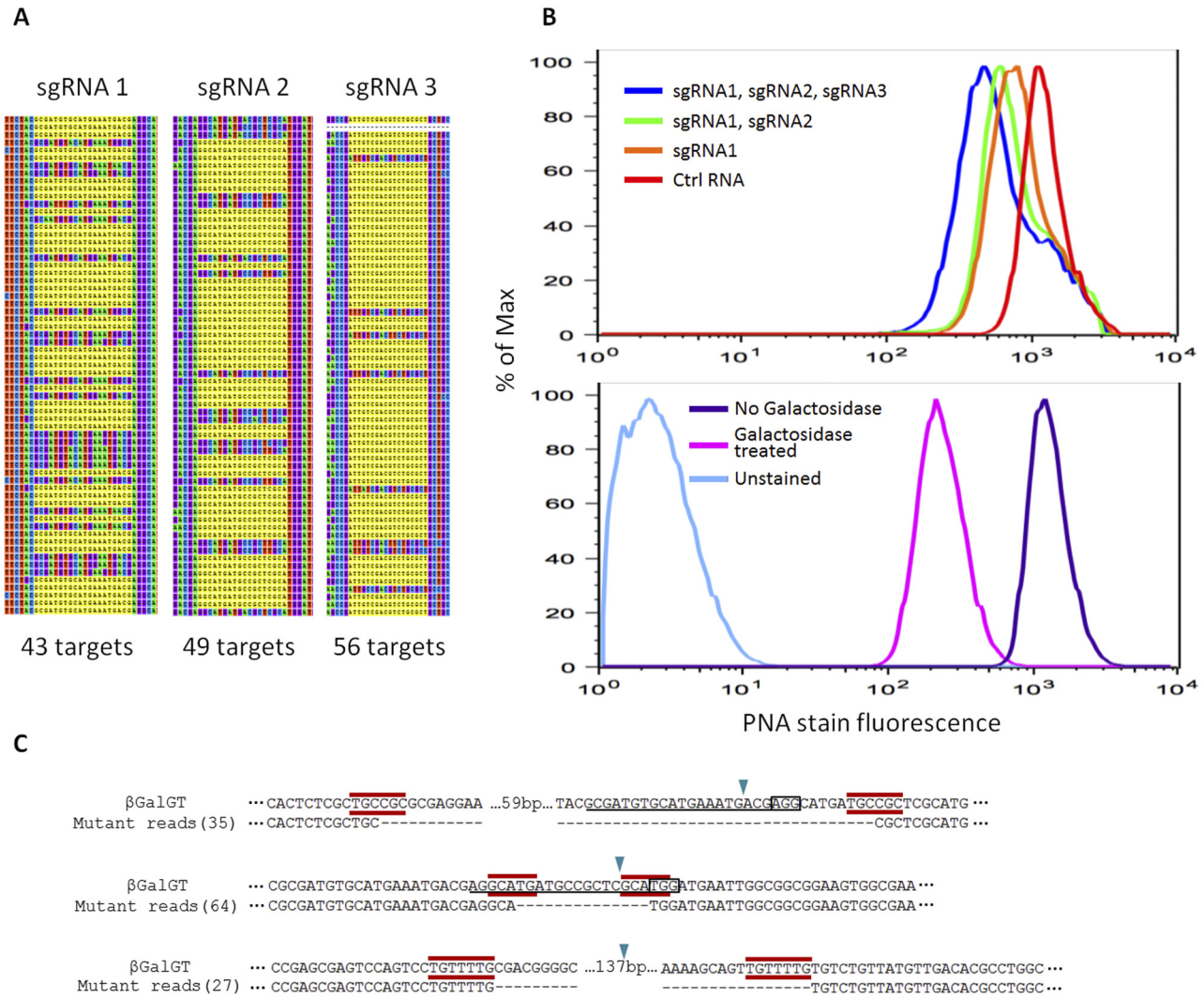

FIG 5 Knockdown of β-GalGT activity by Cas9-mediated gene family mutation. (A) sgRNA targeting strategies for the β-GalGTgene family. DNA alignment at sgRNA targeting regions are shown: highlighted in yellow are sgRNA targeting sequences. sgRNAs 1, 2, and 3 target 43, 49, and 56 out of 65 genes in the gene family, and each gene is targeted by at least one sgRNA. Complete gene identifiers, genome locations, and annotations are presented in Table S3 in the supplemental material. (B) Flow cytometric histograms of PNA-stained *T. cruzi* epimastigotes transfected sequentially with one, two, or three sgRNAs targeting the β-GalGT gene family (top) or treated with β-galactosidase (bottom). PNA binds specifically to β-galactosyl residues and indicates a progressive reduction in surface β-galactosyl residues with each additional sgRNA transfection. Biochemical removal of surface β-galactosyl residues using galactosidase was used as a control for the PNA staining. (C) Genome sequencing reads support novel junctions in the 3 target regions (from top): target site 1, target site 2, and target site 3. Boxed is the PAM (on the reverse strand), red shows microhomology sequences flanking the sgRNA targeting sequence, and the double-stranded cut sites are indicated with blue arrows.

family with as few as 3 sgRNAs (Fig. 5A). We conducted sequential transfections of the 3 guides, assessing surface β-galactosyl residues after each transfection by using a fluorescently labeled peanut agglutinin (PNA) lectin specific for Gal-β(1,3)-GalNAc. Flow cytometric analysis demonstrated progressive reduction in surface β-galactosyl residues with each delivery of an additional sgRNA (Fig. 5B).

To further assess the genome-wide efficiency of β-GalGT mutation and to determine potential off-target mutations induced by Cas9 armed with multiple sgRNAs, we conducted whole-genome sequencing of the uncloned parasite population that had received 3 sgRNAs and compared these results to those with Cas9-expressing cells not receiving sgRNAs. For guide sites 1, 2, and 3, novel junctions indicative of gene deletions were detected in 35, 64, and 27 reads, respectively (Fig. 5C). These reads accounted for 31%, 30%, and 23% of the total reads that mapped to corresponding target regions, indicating that, collectively, 63% of the β-GalGT genes have a deletion in at least one target site. This calculation matches closely to the observed loss of surface galactose residues of approximately 58% determined by lectin staining (Fig. 5B). As with previous single-copy gene targeting by Cas9-sgRNA in *T. cruzi*, the mutations induced were all deletions (of 101, 14, and 162 bp for sites 1, 2, and 3, respectively) and were all associated with regions of microhomology, again supporting MMEJ as the mechanism of repair of DSBs in *T. cruzi* (Fig. 5C).

Potential off-target regions were identified in the genome as sequences that matched to sgRNA targeting sequence with less than 6 mismatches but excluding any mismatches in the proto-

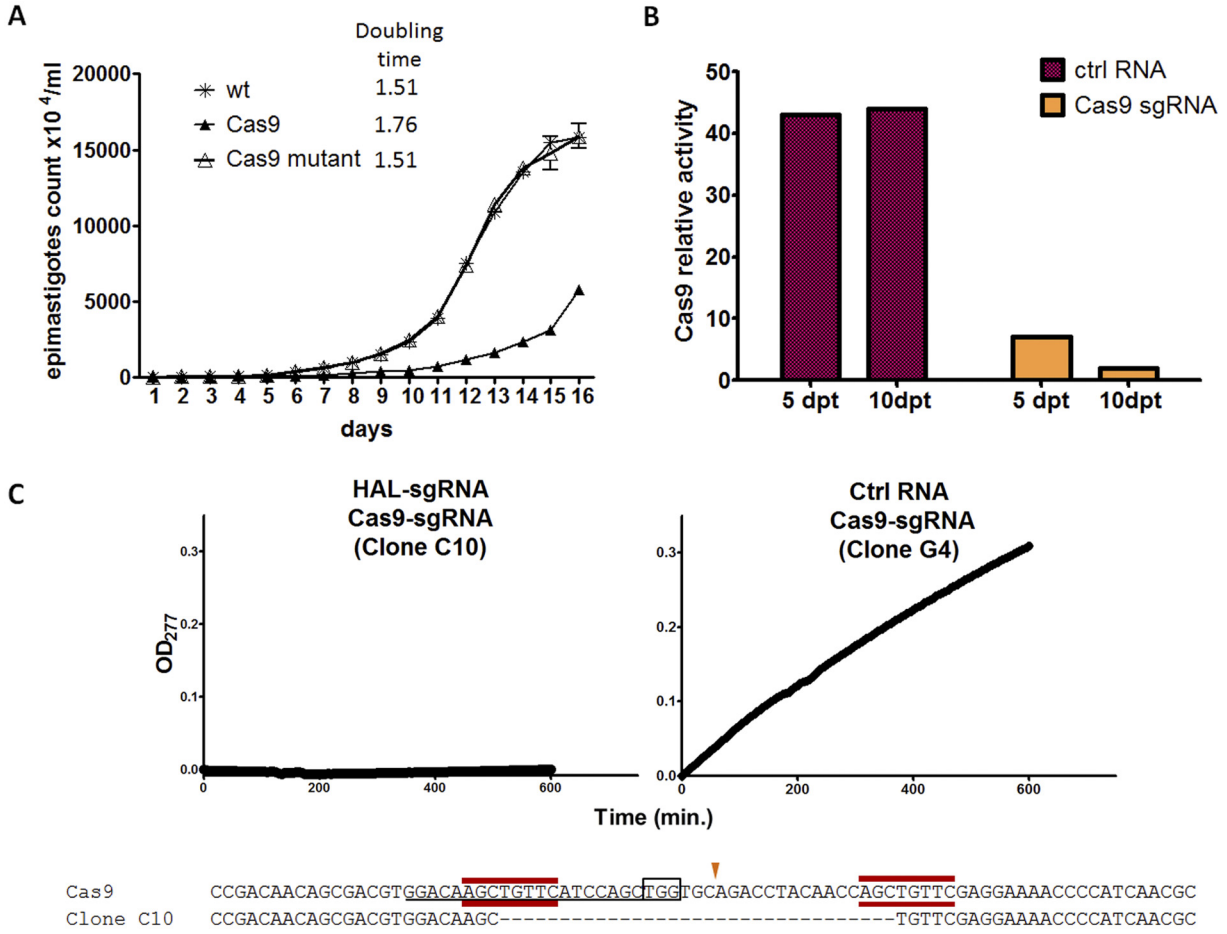

FIG 6 Cas9 expression negatively impacts growth of *T. cruzi* epimastiogtes but could mediate disruption of its own coding sequence. (A) Growth curve of eGFP-labeled epimastigotes that do not express Cas9 (wt), expresses Cas9, or have had Cas9 knocked out by transfecting Cas9-targeting sgRNA. Parasites with stable Cas9 expression had a significantly greater doubling time compared to WT or Cas9-disrupted parasites. (B) Cas9 activity was abolished by 83% and 95% on day 5 and day 10 posttransfection (dpt), respectively, with Cas9-targeting sgRNA, as determined in an eGFP disruption assay, demonstrating that Cas9 could mediate disruption of its own coding sequence. (C) HAL activity determined by rate of urocanic acid formation (measured as the optical density at 277 nm [OD_{277}]) in lysates of clonal epimastigote lines from parasites cotransfected with Cas9 gene-targeting sgRNA, HAL gene-targeting sgRNA, or control (Ctrl) RNA. Sequencing of the Cas9 gene in clone C10, which lacked HAL activity, confirmed the disruption of Cas9, thus demonstrating knockout of both the Cas9 gene and HAL gene in parallel.

spacer adjacent motif (PAM), since this motif is required for Cas9 DSBs (18). By this criterion, all 3 guides have a total of 2 potential off-target sites in the *T. cruzi* genome, and with 100× and 80× coverage in these regions, no mutations in these sites were observed. As deep sequencing read mappers tend to have low tolerance for indels, we used custom perl scripts to search unmapped reads for indels in the 2 possible off-target sites, and again we found no indels supported by >2 similar reads. Thus, we concluded that the multiple genes can be simultaneously mutated in the *T. cruzi* genome without production of detectable off-target mutations.

Impact of Cas9 expression on *T. cruzi* growth. We previously observed that *T. cruzi* lines expressing selected exogenous proteins occasionally have altered growth kinetics. Examination of *T. cruzi* epimastigotes with stable Cas9 expression indicated a substantial increase in doubling time (Fig. 6A). To attempt to rescue WT growth in these Cas9-expressing lines, we designed an sgRNA targeting Cas9 and used these guides to disrupt the Cas9 gene, rapidly returning these lines to wild-type growth (Fig. 6A). Further evidence of the disruption of the Cas9 gene by Cas9-sgRNA-guided Cas9 protein was obtained by the failure of eGFP-sgRNA to alter eGFP expression in the lines transfected with the Cas9 sgRNA (Fig. 6B). Endogenous *T. cruzi* genes and the Cas9 gene can also be simultaneously disrupted. Cotransfection of HAL-sgRNA and Cas9-sgRNA resulted in clones devoid of HAL activity and with defective Cas9 (Fig. 6C). Thus, Cas9 can mediate disruption of its own coding gene, making it possible to perform genome modifications in *T. cruzi* lines expressing Cas9 and simultaneously "killing" Cas9 expression.

DISCUSSION

Understanding the complexities of host-pathogen interactions is greatly facilitated by the ability to manipulate host and pathogen genomes—by gene disruption or by insertion of genes with new or enhanced functions. While manipulation of the *T. cruzi* genome has been possible for some time, the processes to achieve modifications are not rapid, easy, or routine. We previously reported on a multisite Gateway approach for the more facile pro-

duction of constructs for gene disruption in *T. cruzi* (4). However, because of the low rate of homologous recombination and the relatively high resistance of *T. cruzi* to antibiotic selection, production of null mutants of single-copy genes using this approach requires a minimum of several months and the use of multiple antibiotic resistance genes. The limited number of available resistance genes makes knockout of more than 1 or 2 genes unmanageable by this approach. The latter limitation is a particular problem in *T. cruzi*, which has over 100 gene families with 4 or more members and several families that contain hundreds of genes. And, unlike its closest genetic relatives, the African trypanosomes, *T. cruzi* lacks the machinery for inhibitory RNAs (19, 20), making suppression of gene function by RNAi infeasible.

The CRISPR-Cas system has rapidly transformed the speed and ease of gene manipulation for multiple species (5). By adapting CRISPR-Cas9 for use in *T. cruzi*, we were able to quickly and efficiently disrupt endogenous single-copy and multicopy genes, as well as exogenous genes. Because of the high rate of gene mutation when using CRISPR-Cas9 in *T. cruzi*—routinely 60 to 70% double-/multiallelic mutations—the impact of gene disruption can be observed within days when appropriate assays are available (e.g., fluorescence for GFP, enzyme activity for HAL, and fatty acid uptake for FATP) instead of months, as in the case of conventional knockouts. For genes lacking assays that can be applied to a parasite population, the principal limiting factor with CRISPR-Cas-mediated mutation is the time required to generate sufficient numbers of parasites from clones in order to confirm the mutations/phenotypes.

The high efficiency of CRISPR-Cas-induced mutations in *T. cruzi* also means that null mutants in essential genes can be generated and monitored over time as protein activity is lost. Our previous studies suggested that genes involved in fatty acid uptake and β-oxidation (4) are essential in *T. cruzi*. We found further support for that conclusion here with the observation that targeting FATP for mutation results in a population of parasites with decreased FA uptake soon after transfection and a return to normal FA uptake by 2 weeks posttransfection, presumably due to the death of the null mutants in the population.

We also found that CRISPR-Cas9 could greatly facilitate HR between a supplied template and specific locations in the genome. By introducing a DSB via RNA-guided Cas9, we were able to replace a genomic eGFP sequence with a larger tdTomato sequence at a frequency several orders of magnitude greater than in the absence of the DSB. This increased frequency makes feasible a number of additional approaches to manipulation of *T. cruzi*, including the tagging of genes in their endogenous loci and rapid isolation of gene replacement mutants by flow sorting based on a knock-in of a fluorescent protein.

Although in the presence of an appropriate template, HR is observed at a detectable frequency following the introduction of RNA-guided DSBs, mutations resulting from error-prone end joining appear to be the preferred mechanism of repairing these DSBs in *T. cruzi*. For multiple analyzed mutations, we found strong evidence for MMEJ as the mechanism of repair of DSBs in *T. cruzi*. MMEJ has been considered a "backup" pathway for DSB repair in most species but appears to be the primary mechanism in trypanosomes, in which NHEJ is absent (8). MMEJ generally uses 5- to 20-bp regions of microhomology to repair DSBs, in the process leaving deletions between the microhomology regions (21). As such, the deletion size should be predictable, once the specific rules for MMEJ are defined (e.g., the relative contribution of microhomology length and distance from the cut site to the repair), and these data can be employed to more efficiently design sgRNAs (22). There is also increasing appreciation for the role of MMEJ in DSB repair in species where NHEJ dominates (23) and emerging information on the putative components of the MMEJ repair machinery (23, 24). Because NHEJ is naturally absent in *T. cruzi* and other kinetoplastids, these organisms should be especially useful for the further dissection of MMEJ mechanisms. Additionally, knowledge of the components uniquely involved in MMEJ could provide insights into how to minimize this error-prone repair pathway and potentially enhance HR, further optimizing *in situ* genome editing in *T. cruzi*.

The potential for off-target sequence disruption is always a concern when using genome editing tools, including CRISPR-Cas (25). However, because of the compactness and low complexity of the *T. cruzi* genome, and with the aid of the sgRNA finder program we developed for *T. cruzi*, we were able to select highly gene-specific sgRNAs with low sequence identity (<15 bp matches in the 20-bp guide) to other sites in the *T. cruzi* genome. Ensuring that any potential off-target sites also lacked the NGG motifs needed for Cas9 nuclease activity also contributes to minimizing off-target effects. This specificity and the lack of off-target effects were confirmed by analysis of deep sequencing data from parasites exposed to multiple sgRNAs.

A number of studies (26–28) have documented the ability to target more than 1 gene for mutation when using the CRISPR-Cas system. We show here the potential to multiplex CRISPR-Cas to more than 50 genes using a small number of sgRNAs. This experiment is only possible in organisms like *T. cruzi*, which contains large numbers of closely related genes. The *T. cruzi* genome contains a remarkable number of moderate (>20), large (>50), and very large (>500) gene families, and among these are ones encoding the thousands of mucins, mucin-associated proteins, and *trans*-sialdase-like proteins that form a large part of the interface between the parasite and mammalian hosts. Modest expansion of gene families in some organisms has been linked to the potential to succeed in variable environments (29). However, the size of the *trans*-sialidase gene family, its variability in composition among different parasite isolates, and its targeting by the host immune responses all argue that the family may have expanded from the few copies identified in other kinetoplastids to its current size in *T. cruzi* in part as an immune evasion mechanism. Testing of this hypothesis has not previously been possible, due to the lack of functional RNAi or another knockdown/knockout system capable of regulating the expression of hundreds of genes. The demonstration here of the ability to knock down a gene family of 65 members may pave the way for studying these much larger gene families of *T. cruzi*.

CRISPR-Cas has revolutionized genome editing in multiple species, and we have shown here the similar promise for use in the kinetoplastid parasite *T. cruzi*. As already noted, the exclusive dependence on MMEJ for DSB repair and the enormous multiplexing capabilities are observations unique to the CRISPR-Cas system for *T. cruzi* at the current time. Cas9 expression in *T. cruzi* does come at the price of decreased growth potential, a consequence also noted in *Saccharomyces cerevisiae* when Cas9 was highly expressed (30), presumably due to Cas9's ability to bind to DNA at PAMs without sgRNA. But this effect was reversible upon mutation of the *Cas9* gene (using the CRISPR-Cas system itself),

providing the potential to simultaneously mutate endogenous *T. cruzi* genes and *Cas9* by using a mixture of sgRNAs. Hopefully, this study is only the beginning of the exploitation of the CRISPR-Cas system in kinetoplastids.

MATERIALS AND METHODS

Growth, transfection, and cloning of *T. cruzi*. Epimastigotes of the CL strain of *T. cruzi* were cultured at 26°C in supplemented liver digested-neutralized tryptose (LDNT) medium as described previously (4). Unless otherwise indicated, 5×10^6 early-log-phase epimastigotes or recently egressed trypomastigotes were resuspended in 100 μl room temperature human T cell Nucleofector solution (Amaxa AG, Cologne, Germany) and 20 μg sgRNA in a total volume of 15 μl and electroporated using the program U-33 in an Amaxa Nucleofector device. For sequential transfections, parasites were allowed 5 days of recovery time between transfections. For tests of homologous recombination, an additional 10 μg of template DNA was added. The electroporated parasites were cultured in 25-cm^2 cell culture flasks (Corning Inc., Lowell, MA) with 10 ml LDNT medium. To generate *T. cruzi* lines stably expressing eGFP and Cas9, 10 μg linearized pTrex-n-eGFP-Neo plasmid was transfected into epimastigotes by using the protocol described above. A total of 250 mg/ml G418 was added at 24 h posttransfection, and the drug concentration was maintained for 4 weeks (at which point parasites transfected with no DNA were no longer viable), eGFP-positive parasites were then sorted by using a MoFlow cell sorter (Dako-Cytomation, Denmark). Sorted eGFP-positive parasites were transfected with pTrex-b-NLS-hSpCas9, 25 μg/ml blasticidin was added 24 h posttransfection, and the drug concentration was maintained for 4 weeks.

The doubling time of epimastigotes was calculated by fitting an exponential curve to density data from days 1 to 14 of culture by using least squares fitting on the Doubling Time website.

Plasmid construction. The *T. cruzi* pTrex-n-eGFP and pTrex-b-NLS-hSpCas9 plasmids were constructed by subcloning the coding sequence of hSpCas9 from pX330 (26) or eGFP (GenBank accession number JQ693016.1; bp 633 to 1352), respectively, into multiple cloning sites of the pTrex plasmid (9) containing a neomycin phosphotransferase gene (pTrex-n) or blasticidin-S deaminase gene (pTrex-b).

sgRNA preparation. sgRNA targeting sequences were designed using a custom sgRNA design tool (available at https://grna.ctegd.uga.edu) that (i) identifies all potential 20-bp sequences containing an NGG PAM site within the query sequence, (ii) predicts all potential off-target sites for each sgRNA, including those with 5 or fewer mismatches to the sgRNA, (iii) indicates the microhomology pairs flanking the sequences targeted by the identified sgRNA, and (iv) predicts targeting efficiency by using a position-specific nucleotide composition scoring matrix (31). A list of ranked sgRNA targeting sequences is returned based on minimal off-targets and minimal flanking distance of microhomology pairs and maximum length of microhomology sequence. For guide design, sgRNAs that are severely self-complementary, potentially preventing hybridization with target DNA, are eliminated by RNA secondary structure predictions obtained at the website http://rna.tbi.univie.ac.at/cgi-bin/RNAfold.cgi.

sgRNAs were *in vitro* transcribed by using the MEGAshortscript T7 kit (Ambion, Life Technologies) according to the manufacturer's instructions. DNA templates for sgRNA *in vitro* transcription were generated by using PCR to amplify sgRNA scaffold sequence from plasmid pX330 using 5′ primers containing T7 promoter sequence and the above-described designed 20-bp target sequence (see Tables S1 and S2 in the supplemental material). An 80-bp fragment of human 18S rRNA transcribed from pTRI-RNA 18S control template supplied with the MEGAshortscript kit (Life Technologies) was used as control RNA.

Flow cytometry and fluorescence microscopy. Flow cytometric analysis was performed using a CyAn flow cytometer (Beckman Coulter), and data were collected by using the Summit v4.3 software (Beckman Coulter). For single-cell cloning, drug-selected lines were deposited into a 96-well plate at a density of 1 cell/well by using a MoFlow cell sorter (Dako-Cytomation, Denmark) and cultured in 200 μl LDNT supplemented with G418 or blasticidin. Each population from an individual well was considered an individual clone.

Fluorescence microscopy was performed to determine the presence of GFP in intracellular and amastigote-stage *T. cruzi* posttransfection with sgRNA targeting eGFP, using a modification of the protocol described previously (32). Images were acquired with an Applied Precision Delta Vision microscope, and images were deconvolved and adjusted for contrast using the Softworx software (Applied Precision).

ELISA analysis. To determine the relative abundance of Cas9 protein in epimastigotes, serial dilutions of whole-cell lysates (cells lysed by 4 freeze-thaw cycles) were assayed with anti-FLAG M2 monoclonal antibody (1:1,000) and anti-α-tubulin monoclonal antibody (1:500) as a loading standard.

Histidine ammonia lyase assay. Epimastigote-stage parasites (1×10^6) were disrupted by freeze-thawing, and the lysate was incubated in 100 mM Tris-HCl (pH 9.0) and 50 mM $MgCl_2$ buffer for 30 min at 25°C before 100 mM histidine was added. HAL activity was determined based on the rate of urocanic acid formation, which was measured based on absorbance at 277 nm after addition of histidine (33).

BODIPY-labeled fatty acid uptake assay. The uptake of fatty acids by *T. cruzi* epimastigotes was measured using the QBT fatty acid uptake assay kit (Molecular Devices). Briefly, 1×10^7 *T. cruzi* epimastigotes were pelleted from LDNT medium, resuspended in 10 μl phosphate-buffered saline (PBS; pH 7.0), and then 200 μl of reconstituted QBT loading solution was added and the parasites were immediately analyzed by using a CyAn flow cytometer (Beckman Coulter). Flow cytometry data were collected continuously for 200 s. To calculate the rate of fatty acid uptake rate with Summit 4.3 (Beckman Coulter), the continuous data were first converted into discrete data by binning fluorescence intensity data into 4-s intervals and determining the mean fluorescence intensity (MFI) for each bin. Then, MFIs were plotted against the center point time stamp of each bin, and the slope of the trend line was used to calculate the uptake rate.

Galactosidase treatment and PNA staining. *T. cruzi* epimastigotes (1×10^7) were washed twice in PBS and then incubated at 37°C for 1.5 h with 10 U of β-galactosidase (grade VIII from *Escherichia coli*; Sigma-Aldrich) in PBS (pH 7.3) containing 50 mM Tris-HCl, 10 mM 2-mercaptoethanol, and 10 mM $MgCl_2$. To assess surface galactose residues, parasites were incubated with 10 μg/ml PNA-Alexa Fluor 647 conjugate (Life Technologies) in PBS at 37°C for 10 min and analyzed by using a CyAn flow cytometer (Beckman Coulter).

Whole-genome sequencing. Genomic DNA was isolated from *T. cruzi* epimastigotes as previously described (34). The DNA samples were enzymatically sheared to a 150-bp mean fragment size by using the Ion Shear DNA fragmentation kit (Life Technologies) and ligated to barcoded adapters by using the Ion Xpress Plus fragment library kit (Life Technologies) per the manufacturer's instructions. Adapter-ligated DNA was size selected using the Pippen prep apparatus (Sage Biosciences) and quantified by using BioAnalyzer (Agilent) and an ion library quantitation kit (Life Technologies), and the libraries were pooled equally and used to template ion sphere particles by using the Ion PI template OT2 200 kit v2 (Life Technologies), per the manufacturer's instructions. Templated beads were then loaded onto a P1 ion proton sequencing chip and sequenced on the Ion Proton system (Life Technologies). Sequencing reads were mapped to the *T. cruzi* strain CL Brener reference genome (TritrypDB version 5) by using Tmap 4.2 (Life Technologies) with nondefault parameters: a score match of 4 and a pen mismatch of 5. To assess mutations at potential off-target sites, a custom perl script was written to identify novel junctions supported by unmapped reads, briefly, all unmapped reads were first analyzed via BLAST to a reference genome using the BLASTn-short program in the suite BLAST 2/2/29+ with nondefault parameters of reward of 2, penalty of 3, and E value of 0.001. Reads that had greater than 95% overall sequence coverage (coverage gap less than 10 bp)

and a best hit for each alignment segment coming from 2 or more different locations in the genome were considered reads that supported a novel junction.

SUPPLEMENTAL MATERIAL

Supplemental material for this article may be found at http://mbio.asm.org/lookup/suppl/doi:10.1128/mBio.02097-14/-/DCSupplemental.

Figure S1, TIF file, 0.4 MB.
Figure S2, TIF file, 0.4 MB.
Figure S3, TIF file, 0.4 MB.
Figure S4, TIF file, 0.6 MB.
Figure S5, TIF file, 0.5 MB.
Table S1, DOCX file, 0.02 MB.
Table S2, DOCX file, 0.02 MB.
Table S3, DOCX file, 0.01 MB.

ACKNOWLEDGMENTS

We thank Boris Striepen and Michael Terns for productive discussions and valuable suggestions, Gretchen Cooley for technical assistance, and all the members of Tarleton Research Group for helpful suggestions throughout this study. We also thank Julie Nelson of the Center for Tropical and Emerging Global Diseases Flow Cytometry Facility at the University of Georgia and Muthugapatti Kandasamy of the Biomedical Microscopy Core at the University of Georgia for their assistance.

This work was supported by NIH grant R01 AI-089952 to R.L.T.

REFERENCES

1. **El-Sayed NM, Myler PJ, Bartholomeu DC, Nilsson D, Aggarwal G, Tran AN, Ghedin E, Worthey EA, Delcher AL, Blandin G, Westenberger SL, Caler E, Cerqueira GC, Branche C, Haas B, Anupama A, Arner E, Aslund L, Attipoe P, Bontempi E, Bringaud F, Burton P, Cadag E, Campbell DA, Carrington M, Crabtree J, Darban H, da Silveira JF, de Jong P, Edwards K, Englund KT, Fazelina G, Feldblyum T, Ferella M, Frasch AC, Gull K, Horn D, Hou L, Huang Y, Kindlund E, Klingbeil M, Kluge S, Koo H, Lacerda D, Levin MJ, Lorenzi H, Louie T, Machado CR, McCulloch R, McKenna A, Mizuno Y, Mottram JC, Nelson S, Ochaya S, Osoegawa K, Pai G, Parsons M, Pentony M, Pettersson U, Pop M, Ramirez JL, Rinta J, Robertson L, Salzberg SL, Sanchez DO, Seyler A, Sharma R, Shetty J, Simpson AJ, Sisk E, Tammi MT, Tarleton R, Teixeira S, Van Aken S, Vogt C, Ward PN, Wickstead B, Wortman J, White O, Fraser CM, Stuart KD, Andersson B.** 2005. The genome sequence of *Trypanosoma cruzi*, etiologic agent of Chagas disease. Science **309:**409–415. http://dx.doi.org/10.1126/science.1112631.
2. **De Pablos LM, Osuna A.** 2012. Multigene families in *Trypanosoma cruzi* and their role in infectivity. Infect Immun **80:**2258–2264. http://dx.doi.org/10.1128/IAI.06225-11.
3. **Weston D, Patel B, Van Voorhis WC.** 1999. Virulence in *Trypanosoma cruzi* infection correlates with the expression of a distinct family of sialidase superfamily genes. Mol Biochem Parasitol **98:**105–116. http://dx.doi.org/10.1016/S0166-6851(98)00152-2.
4. **Xu D, Brandán CP, Basombrío MA, Tarleton RL.** 2009. Evaluation of high efficiency gene knockout strategies for *Trypanosoma cruzi*. BMC Microbiol **9:**90. http://dx.doi.org/10.1186/1471-2180-9-90.
5. **Sander JD, Joung JK.** 2014. CRISPR-Cas systems for editing, regulating and targeting genomes. Nat Biotechnol **32:**347–355. http://dx.doi.org/10.1038/nbt.2842.
6. **Niu Y, Shen B, Cui Y, Chen Y, Wang J, Wang L, Kang Y, Zhao X, Si W, Li W, Xiang AP, Zhou J, Guo X, Bi Y, Si C, Hu B, Dong G, Wang H, Zhou Z, Li T, Tan T, Pu X, Wang F, Ji S, Zhou Q, Huang X, Ji W, Sha J.** 2014. Generation of gene-modified cynomolgus monkey via Cas9/RNA-mediated gene targeting in one-cell embryos. Cell **156:**836–843. http://dx.doi.org/10.1016/j.cell.2014.01.027.
7. **Burton P, McBride DJ, Wilkes JM, Barry JD, McCulloch R.** 2007. Ku heterodimer-independent end joining in Trypanosoma brucei cell extracts relies upon sequence microhomology. Eukaryot Cell **6:**1773–1781. http://dx.doi.org/10.1128/EC.00212-07.
8. **Glover L, Jun J, Horn D.** 2011. Microhomology-mediated deletion and gene conversion in African trypanosomes. Nucleic Acids Res **39:**1372–1380. http://dx.doi.org/10.1093/nar/gkq981.
9. **Vazquez MP, Levin MJ.** 1999. Functional analysis of the intergenic regions of TcP2β gene loci allowed the construction of an improved *Trypanosoma cruzi* expression vector. Gene **239:**217–225. http://dx.doi.org/10.1016/S0378-1119(99)00386-8.
10. **Fu Y, Sander JD, Reyon D, Cascio VM, Joung JK.** 2014. Improving CRISPR-Cas nuclease specificity using truncated guide RNAs. Nat Biotechnol **32:**279–284. http://dx.doi.org/10.1038/nbt.2808.
11. **Ngô H, Tschudi C, Gull K, Ullu E.** 1998. Double-stranded RNA induces mRNA degradation in Trypanosoma brucei. Proc Natl Acad Sci U S A **95:**14687–14692. http://dx.doi.org/10.1073/pnas.95.25.14687.
12. **Dickinson DJ, Ward JD, Reiner DJ, Goldstein B.** 2013. Engineering the Caenorhabditis elegans genome using Cas9-triggered homologous recombination. Nat Methods **10:**1028–1034. http://dx.doi.org/10.1038/nmeth.2641.
13. **Böttcher R, Hollmann M, Merk K, Nitschko V, Obermaier C, Philippou-Massier J, Wieland L, Gaul U, Förstemann K.** 2014. Efficient chromosomal gene modification with CRISPR/cas9 and PCR-based homologous recombination donors in cultured Drosophila cells. Nucleic Acids Res **42:**e89. http://dx.doi.org/10.1093/nar/gku289.
14. **Auer TO, Duroure K, De Cian A, Concordet JP, Del Bene F.** 2014. Highly efficient CRISPR/Cas9-mediated knock-in in zebrafish by homology-independent DNA repair. Genome Res **24:**142–153. http://dx.doi.org/10.1101/gr.161638.113.
15. **Ghorbal M, Gorman M, Macpherson CR, Martins RM, Scherf A, Lopez-Rubio JJ.** 2014. Genome editing in the human malaria parasite Plasmodium falciparum using the CRISPR-Cas9 system. Nat Biotechnol **32:**819–821. http://dx.doi.org/10.1038/nbt.2925.
16. **Schwank G, Koo BK, Sasselli V, Dekkers JF, Heo L, Demircan T, Sasaki N, Boymans S, Cuppen E, van der Ent CK, Nieuwenhuis EE, Beekman JM, Clevers H.** 2013. Functional repair of CFTR by CRISPR/Cas9 in intestinal stem cell organoids of cystic fibrosis patients. Cell Stem Cell **13:**653–658. http://dx.doi.org/10.1016/j.stem.2013.11.002.
17. **Ran FA, Hsu PD, Lin CY, Gootenberg JS, Konermann S, Trevino AE, Scott DA, Inoue A, Matoba S, Zhang Y, Zhang F.** 2013. Double nicking by RNA-guided CRISPR Cas9 for enhanced genome editing specificity. Cell **154:**1380–1389. http://dx.doi.org/10.1016/j.cell.2013.08.021.
18. **Cho SW, Kim S, Kim Y, Kweon J, Kim HS, Bae S, Kim JS.** 2014. Analysis of off-target effects of CRISPR/Cas-derived RNA-guided endonucleases and nickases. Genome Res **24:**132–141. http://dx.doi.org/10.1101/gr.162339.113.
19. **DaRocha WD, Otsu K, Teixeira SM, Donelson JE.** 2004. Tests of cytoplasmic RNA interference (RNAi) and construction of a tetracycline-inducible T7 promoter system in *Trypanosoma cruzi*. Mol Biochem Parasitol **133:**175–186. http://dx.doi.org/10.1016/j.molbiopara.2003.10.005.
20. **Kolev NG, Tschudi C, Ullu E.** 2011. RNA interference in protozoan parasites: achievements and challenges. Eukaryot Cell **10:**1156–1163. http://dx.doi.org/10.1128/EC.05114-11.
21. **McVey M, Lee SE.** 2008. MMEJ repair of double-strand breaks (director's cut): deleted sequences and alternative endings. Trends Genet **24:**529–538. http://dx.doi.org/10.1016/j.tig.2008.08.007.
22. **Bae S, Kweon J, Kim HS, Kim JS.** 2014. Microhomology-based choice of Cas9 nuclease target sites. Nat Methods **11:**705–706. http://dx.doi.org/10.1038/nmeth.3015.
23. **Ottaviani D, LeCain M, Sheer D.** 2014. The role of microhomology in genomic structural variation. Trends Genet **30:**85–94. http://dx.doi.org/10.1016/j.tig.2014.01.001.
24. **Crespan E, Czabany T, Maga G, Hübscher U.** 2012. Microhomology-mediated DNA strand annealing and elongation by human DNA polymerases lambda and beta on normal and repetitive DNA sequences. Nucleic Acids Res **40:**5577–5590. http://dx.doi.org/10.1093/nar/gks186.
25. **Fu Y, Foden JA, Khayter C, Maeder ML, Reyon D, Joung JK, Sander JD.** 2013. High-frequency off-target mutagenesis induced by CRISPR-Cas nucleases in human cells. Nat Biotechnol **31:**822–826. http://dx.doi.org/10.1038/nbt.2623.
26. **Cong L, Ran FA, Cox D, Lin S, Barretto R, Habib N, Hsu PD, Wu X, Jiang W, Marraffini LA, Zhang F.** 2013. Multiplex genome engineering using CRISPR/Cas systems. Science **339:**819–823. http://dx.doi.org/10.1126/science.1231143.
27. **Wang H, Yang H, Shivalila CS, Dawlaty MM, Cheng AW, Zhang F, Jaenisch R.** 2013. One-step generation of mice carrying mutations in multiple genes by CRISPR/Cas-mediated genome engineering. Cell **153:**910–918. http://dx.doi.org/10.1016/j.cell.2013.04.025.

28. **Jao LE, Wente SR, Chen W.** 2013. Efficient multiplex biallelic zebrafish genome editing using a CRISPR nuclease system. Proc Natl Acad Sci U S A **110:**13904–13909. http://dx.doi.org/10.1073/pnas.1308335110.
29. **Tamate SC, Kawata M, Makino T.** 2014. Contribution of nonohnologous duplicated genes to high habitat variability in mammals. Mol Biol Evol **31:**1779–1786. http://dx.doi.org/10.1093/molbev/msu128.
30. **Ryan OW, Skerker JM, Maurer MJ, Li X, Tsai JC, Poddar S, Lee ME, DeLoache W, Dueber JE, Arkin AP, Cate JH.** 2014. Selection of chromosomal DNA libraries using a multiplex CRISPR system. Elife **3:**03703. http://dx.doi.org/10.7754/eLife.03703.
31. **Doench JG, Hartenian E, Graham DB, Tothova Z, Hegde M, Smith L, Sullender M, Ebert BL, Xavier RJ, Root DE.** 2014. Rational design of highly active sgRNAs for CRISPR-Cas9-mediated gene inactivation. Nat Biotechnol **32:**1262–1267. http://dx.doi.org/10.1038/nbt.3026.
32. **Agrawal S, Dooren GG, Beatty WL, Striepen B.** 2009. Genetic evidence that an endosymbiont-derived endoplasmic reticulum-associated protein degradation (ERAD) system functions in import of apicoplast proteins. J Biol Chem **284:**33683–33691. http://dx.doi.org/10.1074/jbc.M109.044024.
33. **Tabor H, Mehler A.** 1955. Histidase and urocanase. Methods Enzymol **2:**228–233. http://dx.doi.org/10.1016/S0076-6879(55)02193-9.
34. **Minning TA, Weatherly DB, Flibotte S, Tarleton RL.** 2011. Widespread, focal copy number variations (CNV) and whole chromosome aneuploidies in *Trypanosoma cruzi* strains revealed by array comparative genomic hybridization. BMC Genomics **12:**139. http://dx.doi.org/10.1186/1471-2164-12-139.